Performance Comparison of Slit and Nanoporous Graphene Oxide Membranes in Water Desalination

R. M. S. Ferreira,[1] J. P. K. Abal,[2] P. R. B. Côrtes,[3] M. L. Pereira Jr.,[4,5] M. H. Köhler,[6] P. A. Netz,[7] and M. C. Barbosa[8]

[1)] *Federal University of Recôncavo da Bahia, 44380-000, Cruz das Almas, Bahia, Brazil.*
[2)] *VanellusRad, Information Technology & Services, Florianópolis, Santa Catarina, Brazil.*
[3)] *Department of Physics, Institute of Physics and Mathematics, Federal University of Pelotas, 96010-610, Pelotas, Rio Grande do Sul, Brazil.*
[4)] *Departamento de Engenharia Elétrica, Universidade de Brasília, UNB, 70910-900, Brasília, Distrito Federal, Brazil.*
[5)] *Department of Materials Science and NanoEngineering, Rice University, Houston, Texas 77005, United States.*
[6)] *Departamento de Física da Universidade Federal de Santa Maria, UFSM, 97105-900, Santa Maria, Rio Grande do Sul, Brazil.*
[7)] *Instituto de Química da Universidade Federal do Rio Grande do Sul, UFRGS, 91501-970, Porto Alegre, Rio Grande do Sul, Brazil.*
[8)*] *Instituto de Física, Universidade Federal do Rio Grande do Sul, 91501-970, Porto Alegre, Rio Grande do Sul, Brazil.*

(*Electronic mail: rogelma.maria@gmail.com)

(Dated: 8 January 2026)

Graphene oxide (GO) membranes have emerged as promising candidates for water desalination as a result of their structural and transport properties. In this study, we employ fully atomistic classical molecular dynamics simulations to investigate the performance of monolayer GO membranes featuring pore- and slit-like nanostructures. We analyze the influence of the width of the slits, ranging from 0.8 to 1.5 nm, on water transport and salt rejection by monitoring the spatial and temporal distribution of water molecules and ions. Furthermore, we assess the effect of applied pressure on water density profiles and compute the potential of mean force (PMF) for water molecules traversing the slits. Our results reveal that slits offer tunable transport characteristics and that nanopores generally outperform slits in the combined metrics of water flux and ion exclusion at low pressures. At higher pressures, however, 1.0 to 1.5 nm slits exhibit a permeability gain that can exceed comparable nanopore systems, with a reduction in salt rejection, whereas 0.8 nm slits retain near-complete ion exclusion over the range examined. These findings delineate operating regimes in which each architecture is advantageous and guide the optimization of nanostructure design for advanced desalination technologies.

I. INTRODUCTION

Water scarcity stands among the most pressing challenges of the twenty-first century, directly affecting billions of people worldwide. Although water covers more than 70% of the Earth's surface, only about 3% corresponds to freshwater available for human use. This natural limitation is further exacerbated by population growth and climate change, which alter the global hydrological cycle and intensify pressure on water resources. The consequences of these processes extend across critical domains, compromising energy production, food security, public health, and economic development, while also hindering poverty reduction. Owing to its magnitude, water scarcity has been incorporated into international development agendas and is recognized as a central issue for the achievement of the Sustainable Development Goals[1].

Desalination has emerged as a viable response to this scenario and, since the 1960s, has undergone technological improvements that have reduced the energy consumption per cubic meter of water produced while also enhancing reliability and cost-effectiveness[2–7]. Among available technologies, reverse osmosis (RO) is the most widely adopted. However, it remains more energy-intensive than conventional freshwater treatment methods due to the thermodynamic limitations intrinsic to the separation of saline solutions. Progress toward the theoretical minimum energy consumption is therefore expected to yield substantial long-term savings and strengthen the sustainability of RO based desalination systems[8–11].

In parallel with these developments, advances in nanomaterials have driven the design of more efficient membranes for desalination[12–18]. The performance of such membranes depends on the balance between water permeability and salt rejection, properties strongly influenced by surface charge distribution, pore geometry, and applied pressure. In our previous work, we investigated nanoporous molybdenum disulfide (MoS_2) membranes, which combine high water permeation with significant ion rejection[19–23]. We also found that the organization of charges around the pore plays a decisive role, since charge-free analogs of MoS_2 can, for specific pore diameters, yield higher water flux than conventional MoS_2[21].

Graphene and graphene oxide (GO) represent another important class of materials for desalination membranes[24–30]. In these systems, the pore entrance chemistry exerts direct control over transport properties. In graphene, pores with diameters between 0.7 and 0.8 nm display marked differences, as hydrogenated entrances promote higher permeability but lower salt rejection compared with hydroxylated ones[31]. In

GO membranes with pore diameters between 0.6 and 0.8 nm, the opposite trend has been reported, with hydrogenated entrances producing lower permeability and higher rejection relative to hydroxylated counterparts[32]. Despite these contrasting behaviors, hydroxylated graphene pores tend to outperform those of GO in terms of ion rejection, albeit with lower flux[32]. These results highlight the interplay of two mechanisms. The first arises from the chemical nature of surface functional groups, hydrophobic in graphene and hydrophilic in GO, which makes the latter more attractive to both water and ions. The second is related to the charge distribution at the pore entrance, which facilitates transport in graphene but induces a more ordered water structure in GO, thereby reducing flow.

Beyond surface chemistry, channel geometry also exerts a decisive influence on membrane performance[33–36]. Studies of water flow through nanoslits in monolayer graphene have shown that both flux and permeability vary with applied pressure and slit width[37–40]. Yamada and Matsuzaki[37] reported a threshold near $d = 0.8$ nm, above which water molecules cease to permeate in a single layer and begin to form multiple layers. For MoS_2 slits, however, this behavior is not observed, and the presence of charges at the entrance is sufficient to promote transport[41]. Although recent advances have demonstrated that structural reorganization strategies in GO membranes, such as vertical lamellar alignment, can reduce channel tortuosity and enhance permeability[42], the specific role of nanoslits in governing water and ion transport remains largely unexplored. Given that nanopores in graphene and GO exhibit distinct permeabilities at the nanoscale, it becomes relevant to ask whether water flow and salt rejection through a nanoslit in graphene would differ from those in GO.

Recent studies have shown that surface charge distribution is a key factor controlling water and ion transport in graphene membranes. Guardiani and colleagues demonstrated that the asymmetry of ion distributions and the orientational effects induced by the applied potential and pore charge significantly affect conduction[43]. The charged pore surfaces can strongly slow down water dynamics, emphasizing the role of electrostatics in confined transport[44]. For GO, the spatial arrangement of functional groups governs counter ion accumulation and co ion exclusion, meaning that even chemically similar slits in graphene and GO can exhibit distinct transport properties. These findings indicate that differences in charge topology between graphene and GO nanoslit membranes naturally lead to different water flow regimes and salt rejection efficiencies[45].

In this context, since pores in graphene and GO membranes exhibit distinct permeabilities at the nanoscale, it is reasonable to question whether water flow and salt rejection through a nanoslit in a graphene membrane would differ from those in an oxidized graphene membrane. In this work, we address this question through fully atomistic classical molecular dynamics simulations (MD), assessing the ability of monolayer GO membranes to separate salt from water efficiently. We compare slit-like and pore-like nanostructures, with emphasis on how to slit size influences water mobility and ion rejection dynamics.

The remainder of the paper is organized as follows. Section 2 presents the methods and simulation details; in Section 3, we discuss the results and in Section 4, we present the conclusions and remarks.

II. METHODS AND SIMULATION DETAILS

In this section, we describe the computational model employed to investigate water transport through nanoslits in GO membranes. The system was designed to represent two confined reservoirs separated by a GO membrane, enabling the simultaneous evaluation of water flux and ion rejection for different slit widths.

The simulation box was initially constructed with dimensions of 4.70 nm $\times$ 4.69 nm $\times$ 70 nm along the x, y and z directions, respectively. The membrane was placed at the center of the box, separating one reservoir filled with pure water from another containing saline solution. Graphene walls were used as pistons to control the pressure applied to the solutions. A view of the central GO slit is shown in Figure 1. The pure water reservoir contained 2784 molecules. The saline reservoir, had its salt concentration determined from the total number of ions in solution N_{ions}, the number of water molecules N_{H_2O}, and the molar mass of water M_{H_2O}[46], expressed as

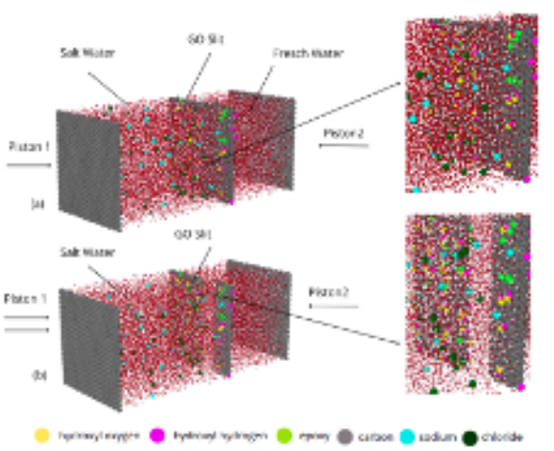

FIG. 1. System with a central GO membrane and two reservoirs, considered without (a) and with (b) the presence of a nanoslit.

$$[\text{NaCl}] = \frac{N_{\text{ions}} \times 10^3}{2 \times N_{H_2O} \times M_{H_2O}}. \quad (1)$$

The division by two accounts for the ion pair, while $M_{H_2O} = 18$ g mol^{-1}. In this work the salt concentration was 0.33 mol/kg corresponding to 90 ions for 7515 water molecules taking into account the combination of the two reservoirs.

The GO membrane was generated from a flat graphene sheet functionalized with hydroxyl and epoxy groups at an oxidation level of 20%. Three different slit widths were considered, denoted L_1 (0.8 nm), L_2 (1.0 nm) and L_3 (1.5 nm), as illustrated in Figure 2.

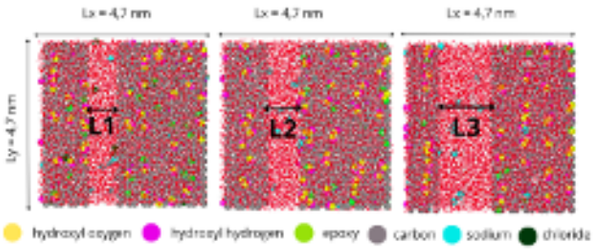

FIG. 2. Illustration of the GO membrane for three different slit diameters: $L_1 = 0.8\,nm$, $L_2 = 1.0\,nm$ and $L_3 = 1.5\,nm$.

The simulations were performed with the Large scale Atomic Molecular Massively Parallel Simulator (LAMMPS) package[47]. Several preparation stages were necessary before the transport simulations. The system was first constructed with all molecules and the membrane arranged in layers, and the GO membrane was initially considered without a slit. The model was then subjected to an energy minimization for 150 ps in the NVE ensemble to relax atomic positions.

Initial velocities were assigned randomly so that the starting temperature of the system was 10 K, a low value chosen to avoid abrupt changes during this phase. Afterward, the system was equilibrated under the NVT ensemble at 300 K. During these steps, the membrane remained fixed, by imposing positional restraints to the carbon atoms of the plane, preventing global membrane motion. The functional groups (epoxy, hydroxyl, and carbon), however, were not constrained and were allowed to fluctuate around their equilibrium positions.

The system was to thermalize water molecules and ions at room temperature. Subsequently, external forces were applied to the piston atoms along the z direction, pushing toward the GO membrane until the reservoirs equilibrated at the target water density of 1 g/cm^3.

Once the system was thermalized and equilibrated at room temperature and a density of 1 g/cm^3, we simulated water transport through the slit under applied pressure. At this stage, the nanoslit was opened, and the forces applied to the piston-like carbon walls were adjusted to generate a pressure gradient. The applied pressure was computed from the system cross-sectional area, ensuring a controlled directional flow through the slit. The membrane was kept fixed in space, and additional constraints restricted piston motion to the z direction. The simulations were performed for 6 ns, corresponding to 12 million timesteps. Periodic boundary conditions were applied in all directions, and the equations of motion were integrated with the Velocity-Verlet algorithm[48] using a time step of 0.5 fs. Temperature control was enforced with a Nosé-Hoover thermostat[49,50].

Water molecules were described with the SPC/E (Extended Simple Point Charge) model, a rigid three-site force field with an average polarization correction that reproduces experimental densities and diffusion constants[51] as illustrated in Table I. Ion-ion and ion-water interactions were modeled with the NaCl/ε force field, parameterized to reproduce thermodynamic, structural, and dynamic properties of sodium chloride in aqueous solution when combined with non-polarizable water models[46].

The membrane parametrization was obtained from reference[32], allowing us to compare the behavior of water flow through nanopores and nanoslit using the same force field, as illustrated in Table I. The test the accuracy of the pore simulation, we performed simulations to the 1.0 nm pore under pressures of 300 and 800 bar. Our results are consistent with those reported in reference[32].

All particle interactions were represented by the combined contributions of Lennard-Jones (LJ)[52] and Coulomb terms. The pair potential is expressed as

$$U = \sum_{i<j} \left[4\varepsilon_{ij} \left(\left(\frac{\sigma_{ij}}{r_{ij}} \right)^{12} - \left(\frac{\sigma_{ij}}{r_{ij}} \right)^{6} \right) + \frac{q_i q_j}{4\pi\varepsilon_0 r_{ij}} \right] \qquad (2)$$

where σ and ε are the Lennard-Jones (LJ) interaction parameters between different atoms, q_i is the charge on site i and r_{ij} is the distance between the charge sites i and j.

The long-range Coulomb interactions are calculated by the Particle-Particle Particle-Mesh (PPPM) algorithm[53]. Details on the LJ parameters are shown in Table I.

TABLE I. Force Field Parameters

Atom	σ (Å)	ε (kcal/mol)	Charge (e)
C [32]	3.3997	0.0694	+0.1966
O (epoxy) [32]	3.166	0.1399	-0.5260
O (Hydroxyl) [32]	2.9	0.1492	-0.4
H (Hydroxyl) [32]	0	0	+0.3294
O (SPC/E) [51]	3.166	0.1553	-0.8476
H (SPC/E) [51]	0	0	+0.4238
Na^+ ε [46]	2.52	0.0346568	+0.885
Cl^- ε [46]	3.85	0.382437	-0.885

The flow of water across the membrane is determined using the specific permeability of the membrane:

$$A_m = \frac{\phi}{(P - \Pi)} \qquad (3)$$

which incorporates information about the slit density and the membrane resistance to water flow. In this expression, ϕ is the water flux expressed in L/hm^2 (liters per square meter per hour), P and Π are the applied pressure and the osmotic pressure, respectively. Membrane permeability is defined as the ratio of flux to applied pressure difference, with dimensions of $LMH/$ bar or $Lm^{-2}h^{-1}P^{-1}$ [21].

Figure 3 presents snapshots of the simulations of the flow of water through slits in a graphene oxide (GO) membrane. The images show three distinct slit widths.

III. RESULTS AND DISCUSSION

To evaluate the efficiency of GO membranes for desalination, we first examined the water flux, defined as the number

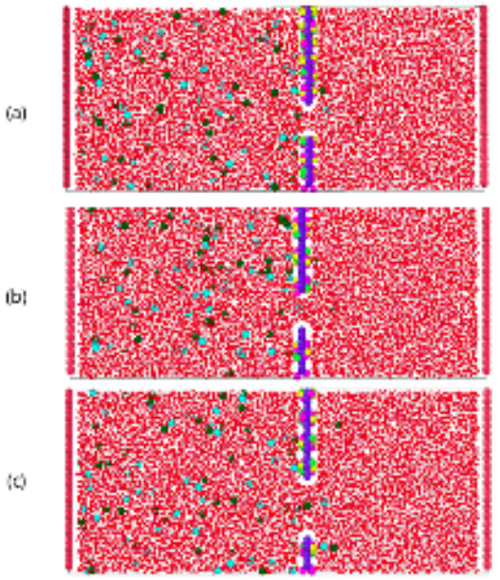

FIG. 3. Snapshots of flows through slit in oxide graphene (GO) membrane. (a) Slit width of $L_1 = 0.8nm$, (b) Slit width of $L_2 = 1.0nm$ and (b) Slit width of $L_3 = 1.5nm$.

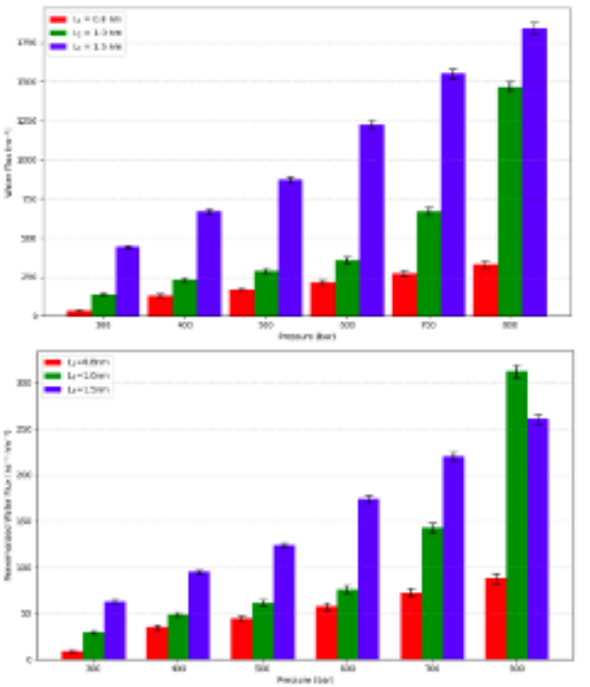

FIG. 4. Absolute flux (top panel) and area-normalized flux (bottom panel) of water as a function of different applied pressures for slit widths $L_1 = 0.8$ nm, $L_2 = 1.0$ nm, and $L_3 = 1.5$ nm. Error bars are the deviation from the mean value.

of water molecules crossing the slits (L_1, L_2, and L_3, separately) as a function of time under an applied pressure. Figure 4 presents these results and shows that the flux increases with slit width, as expected. Among the slit widths investigated, water mobility increases linearly with pressure for the 0.8 nm and 1.5 nm cases, while an exponential increase is observed for the 1.0 nm slit. At high pressures, the L_2 slit exhibits the highest normalized water flux, surpassing even the L_3 slit, which can be attributed to an optimized balance between confinement and channel size. Narrower slits such as L_1 are hindered by stronger wall-water interactions and restricted molecular rearrangements, limiting pressure-driven transport. In contrast, wider slits such as L_3 allow greater configurational freedom. However, part of the applied pressure is dissipated through internal friction and less ordered transport, which reduces the flux per unit area. The water flux computed from the slope of Figure 4, was obtained for each pressure and slit size and the results are summarized in Table II.

TABLE II. Water flux for different oxide graphene slit sizes with associated uncertainties.

Pressure (bar)	$L = 0.8nm$	$L = 1.0nm$	$L = 1.5nm$
300	33.7 ± 5.8	137.86 ± 8.5	442.64 ± 10.7
400	129.5 ± 10.1	229.99 ± 12.3	668.52 ± 14.5
500	167.19 ± 12.3	287.99 ± 15.2	871.48 ± 18.1
600	215.89 ± 15.2	356.49 ± 20.5	1226.2 ± 25.8
700	272.19 ± 18.5	669.99 ± 25.7	1552.5 ± 30.4
800	330.50 ± 20.6	1466.66 ± 30.8	1840.5 ± 35.7

The intermediate width L_2 maximizes transport efficiency under strong confinement by promoting ordered layering of water molecules while benefiting from slip-flow effects, thereby minimizing viscous dissipation and enhancing permeability per unit area. Comparable optimal-size effects under nanoconfinement have been reported in molecular dynamics studies of water flow through graphene nanoslits, where specific channel widths were found to maximize slip length and volumetric flux at elevated pressures[54]. These findings indicate that under high-pressure conditions, the most efficient transport is achieved for the L_2 case.

After establishing the characteristics of water flux through GO membranes, we extend the analysis to compare slits with nanopores. In this context, Hosseini, Azamat, and Erfan-Niya[32] investigated the performance of water desalination using ultrapermeable functionalized graphene oxide membranes. Their results indicated that flux increases with both applied pressure and pore diameter, for nanopores functionalized with either hydrogenated (hydrophobic) or hydroxylated (hydrophilic) groups. For a nanopore with hydrogenated groups on the surface, with a radius of 4.5 Å and an area of 63.61 Å^2, they reported that the flux under an applied pressure of 300 bar is approximately 30 molecules/ns[32]. To ensure a fair comparison, we calculated the renormalized flux of the slit by dividing it by the number of pores that could fit in the same slit area, according to

$$\text{Flux}_{renorm} = \frac{\text{Flux}_{slit}}{\#\text{pores}} \tag{4}$$

where #pores is the number of pores that can be accommodated within a slit. If the ratio $\text{Flux}_{renorm}/\text{Flux}_{pore}$ is larger than one, the slit is more efficient than the equivalent system

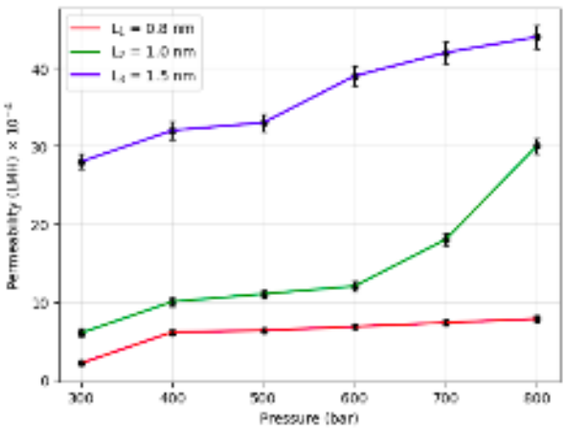

FIG. 5. Water permeability as a function of pressure for slit widths $L_1 = 0.8$ nm, $L_2 = 1.0$ nm and $L_3 = 1.5$ nm. Error bars smaller than the point are not shown.

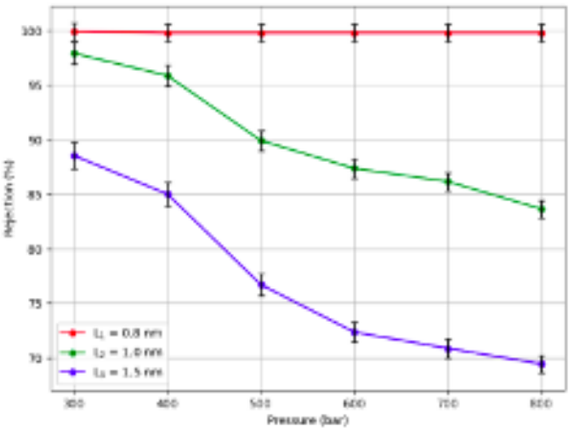

FIG. 6. Salt rejection as a function of pressure for slit widths of 0.8 nm, 1.0 nm, and 1.5 nm.

of pores. Otherwise, the pores remain more efficient.

Table III shows that at 300 bar only the largest slit (1.5 nm) is more efficient than the equivalent pore system, whereas at 800 bar all slits surpass the pores. This indicates that slits become increasingly favorable at higher pressures.

For hydroxylated pores, with a radius of 4.1 Å and an area of 52.81 Å^2, Hosseini and co-authors[32] reported a flux of approximately 40 molecules/ns at 300 bar and 60 molecules/ns at 800 bar.

Table IV shows that for hydroxylated pores at 300 bar all renormalized slit fluxes remain lower than the equivalent pore flux, indicating that pores are more efficient under moderate pressures. At 800 bar, however, the two largest slits (1.0 nm and 1.5 nm) outperform hydroxylated pores, suggesting that slit geometries become advantageous only at higher pressures in this case as well.

Once the characteristics of water flow in GO membranes were examined, it is also important to evaluate the permeability of the systems with slits and equivalent pores at high pressures to assess the efficiency of these membranes for desalination fully.

The water permeability across GO membranes for each slit size is presented in Figure 5. For all cases, at very low pressures, permeability increases linearly with pressure. As the pressure rises, however, the three systems display markedly different behaviors. The water permeability computed from the slope of Figure 5, was obtained for each pressure and slit size and the results are summarized in Table V.

For the 0.8 nm slit, under intermediate and high pressures, permeability remains nearly constant and the curve appears flat with only a slight increase at very high pressures. This behavior is consistent with previous reports on graphene nanoslits[37]. Such a regime can be attributed to the formation of highly ordered water structures that are quasi-crystalline or monolayer-like. Molecules are strongly correlated and exhibit limited mobility. Under this extreme confinement, even as pressure increases, the molecules lack the freedom to rearrange and flow more effectively[55].

For the 1.0 nm and 1.5 nm slits, permeability presents two distinct regimes. Between 400 bar and 600 bar for the 1.0 nm slit, and between 400 bar and 500 bar for the 1.5 nm slit, permeability remains nearly constant with pressure, corresponding to a quasi-crystalline water structure. Above these thresholds, however, the slits are sufficiently broad to enable water molecules to reorganize and flow more efficiently, resulting in a parabolic increase in permeability. Consequently, permeability rises with pressure as shown in Figure 5.

Another important aspect in desalination is the ability of the membrane to reject salt. Figure 6 shows the salt rejection for the three slit widths studied. Rejection is nearly 100% for all pressures in the case of the smallest slit $L_1 = 0.8$ nm. Hydrated ions do not approach the slit, and their absence results in a constant permeability. The salt reject computed from the slope of Figure 6, was obtained for each pressure and slit size and the results are summarized in Table VI.

For the slits $L_2 = 1.0$ nm and $L_3 = 1.5$ nm, salt rejection is 100% at low pressures, but as pressure increases, ions pass through the slit and rejection decreases. Water permeability then rises, as shown in Figure 5, since hydration water is transported along with the ions and adds to the bulk water that does not cross the slit. For nanopores in GO membranes[32], salt rejection also decreases with pressure. In this case, however, ion passage through small pores involves the loss of part of the hydration shell, which reduces water permeability. This explains why at high pressures, slits exhibit higher fluxes than nanopores.

Finally, the Potential of Mean Force (PMF) is employed to describe the energy required to move a water molecule along the z direction. It is computed at equilibrium by the following expression[7,56]

$$\mathrm{PMF}(z) = -k_B T \ln\left[\frac{\rho(z)}{\rho_0}\right], \tag{5}$$

where $\rho(z)$ is the local density, ρ_0 is the bulk density, T is the temperature and k_B is the Boltzmann constant.

Figure 7 presents the PMF profile of the oxygen atoms of water as a function of distance from the membrane center,

TABLE III. Comparison between hydrogenated pores and slits at 300 and 800 bar (in red the case in which the slit is more efficient).

System	Width/Diameter (nm)	Area (nm^2)	Pores	Pressure (bar)	Flux (ns^{-1})	Flux/Flux$_{pore}$	Flux$_{renorm}$/Flux$_{pore}$
Pore-H[32]	0.9	0.63	1	300	30	1	1
Pore-H[32]	0.9	0.63	1	800	48	1	1
L_1	0.8	3.76	6	300	50	1.67	0.28
				800	350	7.3	1.21
L_2	1.0	4.70	7.5	300	137	4.57	0.61
				800	1450	30.2	4.03
L_3	1.5	7.05	11.2	300	450	15	1.34
				800	1850	38.5	3.44

TABLE IV. Comparison between hydroxylated pores and slits at 300 and 800 bar (in red the case in which the slit is more efficient).

System	Width/Diameter (nm)	Area (nm^2)	Pores	Pressure (bar)	Flux (ns^{-1})	Flux/Flux$_{pore}$	Flux$_{renorm}$/Flux$_{pore}$
Pore-OH[32]	0.82	0.52	1	300	40	1	1
Pore-OH[32]	0.82	0.52	1	800	60	1	1
L_1	0.8	3.76	7.12	300	70	1.75	0.25
				800	350	5.83	0.81
L_2	1.0	4.70	8.9	300	137	3.42	0.38
				800	1450	24.17	2.71
L_3	1.5	7.05	13.3	300	450	11.25	0.85
				800	1850	30.83	4.37

TABLE V. Water permeability for different oxide graphene slit sizes with associated uncertainties.

Pressure (bar)	$L = 0.8nm$	$L = 1.0nm$	$L = 1.5nm$
300	2.1 ± 0.2	6.0 ± 0.5	28 ± 3.7
400	6.1 ± 0.3	10 ± 0.7	32.0 ± 3.5
500	6.3 ± 0.3	11 ± 0.7	33.0 ± 1.0
600	6.8 ± 0.8	12 ± 1.0	39.0 ± 7.2
700	7.3 ± 0.4	18 ± 1.2	42 ± 8.4
800	7.0 ± 0.4	30.0 ± 1.5	44.0 ± 8.7

TABLE VI. Salt rejection for different slit sizes with associated uncertainties.

Pressure (bar)	L = 0.8 nm	L = 1.0 nm	L = 1.5 nm
300	99.9 ± 10.2	97.91 ± 10.2	88.53 ± 10.3
400	99.8 ± 10.3	95.86 ± 10.4	85.00 ± 10.4
500	99.8 ± 10.8	89.91 ± 10.8	76.70 ± 10.9
600	99.8 ± 10.9	87.36 ± 10.9	72.35 ± 11.2
700	99.8 ± 11.8	86.16 ± 11.8	70.87 ± 11.9
800	99.8 ± 11.9	83.65 ± 11.9	69.44 ± 11.9

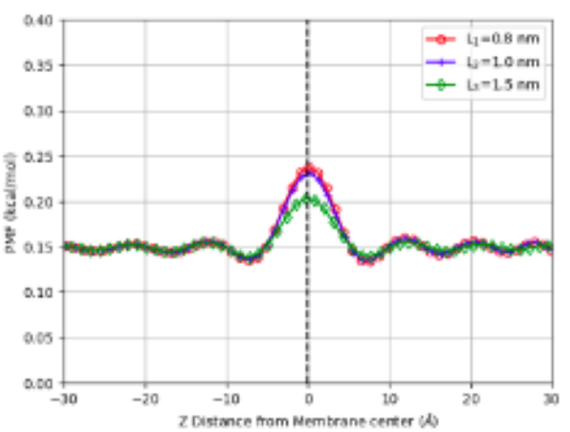

FIG. 7. Potential of Mean Force for oxygen atoms of water along the z axis, centered at the slit of a graphene oxide membrane, for slit sizes of 0.8, 1.0, and 1.5 nm.

taken at $z = 0$. The peak at the center of the slit reveals an energy barrier that prevents the passage of water molecules. This barrier is most pronounced in the narrowest slit of 0.8 nm and decreases as the slit widens. The behavior can be attributed not only to spatial restriction but also to the partial disruption of the hydrogen-bond network in confined regions. In narrower slits, confinement geometry reduces the ability of molecules to preserve their hydrogen bonding, increasing local free energy. In wider slits, this cooperative network is better maintained, resulting in smoother PMF profiles and lower energetic costs for displacement. The PMF of the salt ions is illustrated in the Figure 8. The figure shows that for larger slits the density of salt is almost transparent to the presence of the membrane. This is consistent with our observation of the larger slits not being good for salt rejection.

IV. CONCLUSIONS

In this work, we employed fully atomistic classical molecular dynamics simulations to investigate the transport properties of graphene oxide membranes containing slit and pore nanoarchitectures. By systematically varying the slit widths from 0.8 to 1.5 nm, we characterized the water flux, perme-

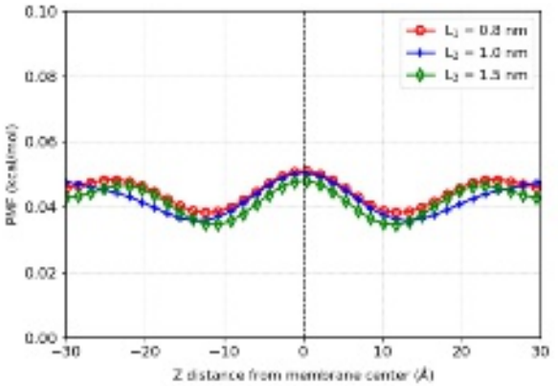

FIG. 8. Potential of Mean Force for sodium atoms of salt along the z axis, centered at the slit of a graphene oxide membrane, for slit sizes of 0.8, 1.0, and 1.5 nm.

ability, salt rejection, and potential of mean force. The results demonstrate that slit geometries provide an adjustable transport response that differs significantly from nanopores, and their relative efficiency depends strongly on the applied pressure regime.

At low pressures, nanopores exhibit superior performance compared to slits when water flux and ion rejection are considered simultaneously. Hydrogenated and hydroxylated pores display higher normalized performance than equivalent slits at 300 bar, reflecting the strong influence of surface chemistry and confinement on water mobility. In contrast, at higher pressures, the behavior reverses. Slits with widths of 1.0 and 1.5 nm show a gain in permeability that surpasses nanoporous systems, although this improvement occurs at the expense of reduced salt rejection. The intermediate slit of 1.0 nm emerges as the most efficient configuration under strong confinement, balancing the ordering of water layers with reduced viscous dissipation. In comparison, the narrow slit of 0.8 nm consistently achieves nearly complete ion exclusion across the entire pressure range investigated.

The analysis of water permeability revealed distinct transport regimes. Narrow slits maintain nearly constant permeability at intermediate and high pressures, a behavior associated with the formation of quasi-crystalline or monolayer-like water structures. Wider slits, however, allow molecular rearrangements under high pressure, which leads to a parabolic increase in permeability. The analysis of salt rejection confirmed the trade-off between permeability and ion exclusion, with rejection decreasing as pressure increases for wider slits. In contrast, the narrow slit effectively blocks hydrated ions under all conditions. Calculations of the potential of mean force corroborated these findings by showing pronounced energy barriers in narrow slits and progressively lower barriers in wider channels, reflecting the breaking and partial preservation of the hydrogen bonding network of water.

Taken together, these results delineate operational regimes in which each membrane architecture becomes advantageous. Nanopores are preferable under moderate pressures when high ion rejection is required. At the same time, slits are more effective under elevated pressures, offering enhanced water permeability and, in some cases, competitive ion rejection. This comparative analysis underscores the importance of tailoring nanoarchitecture geometry to optimize desalination membranes, offering design guidelines for the development of advanced graphene oxide-based systems. Future research can extend these insights by exploring multilayer arrangements, functional group modifications, and coupling with external stimuli, thereby advancing the role of graphene oxide membranes in sustainable desalination technologies.

ACKNOWLEDGMENTS

This work is funded by the Conselho Nacional de Desenvolvimento Científico e Tecnológico (CNPq). The authors acknowledge the National Laboratory for Scientific Computing (LNCC/MCTI, Brazil) and CENAPAD-SP (Centro Nacional de Processamento de Alto Desempenho em São Paulo) for the HPC resources. M.L.P.J. acknowledges financial support from FAPDF (grant 00193-00001807/2023-16), CNPq (grants 444921/2024-9 and 308222/2025-3), and CAPES (grant 88887.005164/2024-00). M.C.B. and M.H.K. thank CNPq Universal grant nr. 405479/2023-9. P.A.N. Acknowledges financial support from CNPq grant 307106/2021-7. This work was carried out with the support of the Coordination for the Improvement of Higher Education Personnel - Brazil (CAPES) - Financing Code 001.

DATA AVAILABILITY STATEMENT

The data that support the findings of this study are available from the corresponding author upon reasonable request.

V. REFERENCES

[1]UNESCO, "The united nations world water development report 2020; water and climate change," (2020).
[2]V. G. Gude, "Desalination and water reuse to address global water scarcity," Rev. Environ. Sci. Biotechnol **16(4)**, 591–609 (2017).
[3]B. Zolghadr-Asli, N. McIntyre, S. Djordjevic, R. Farmani, and L. Pagliero, "A closer look at the history of the desalination industry: the evolution of the practice of desalination through the course of time," Water Supply **23**, 2517–2526 (2023).
[4]M. A. Ahmed, S. A. Mahmoud, and A. A. Mohamed, "Nanomaterials-modified reverse osmosis membranes: a comprehensive review," RSC Adv. **14**, 18879–18906 (2024).
[5]H. Jain, "Optimising the effectiveness of osmotic desalination process by using graphene-based nanomaterials," Discover Water **4**, 68 (2024).
[6]Y. A. Tayeh, "A comprehensive review of reverse osmosis desalination: Technology, water sources, membrane processes, fouling, and cleaning," Desal. Water Treat. **320**, 100882 (2024).
[7]Z. Cao, V. Liu, and A. B. Farimani, "Why is single-layer mos_2 a more energy efficient membrane for water desalination?" ACS Energy Lett. **5**, 2017–2022 (2020).
[8]L. F. Greenlee, D. F. Lawler, B. D. Freeman, B. Marrot, and P. Moulin, "Reverse osmosis desalination: Water sources, technology, and today's challenges," Water Res. **43**, 2317–2348 (2009).

[9]S. Lin and M. Elimelech, "Staged reverse osmosis operation: Configurations, energy efficiency, and application potential," Desalination **366**, 9–14 (2015).
[10]A. A. Moneer and M. M. Elewa, "The innovative technologies for desalination and their cost benefits," Egypt. J. Aquat. Res. **50**, 431–446 (2024).
[11]A. Shabib, B. Tatan, Y. Elbaz, A. A. Hassan, M. A. Hamouda, and M. A. Maraqa, "Advancements in reverse osmosis desalination: Technology, environment, economy, and bibliometric insights," Desalination **598**, 118413 (2025).
[12]Y. H. Teow and A. W. Mohammand, "New generation nanomaterials for water desalination: A review," Desalination **451**, 2–17 (2019).
[13]F. E. Ahmed, A. Khalil, and N. Hila, "Emerging desalination technologies: Current status, challenges and future trends," Desalination **517**, 115183 (2021).
[14]R. Sirohi, Y. Kumar, A. Madhavan, N. A. Sagar, R. Sindhu, B. Bharathiraja, H. O. Pandey, and A. Tarafdar, "Engineered nanomaterials for water desalination: Trends and challenges," Environ. Technol. Innov. **30**, 103108 (2023).
[15]S. Wu, L. E. Peng, Z. Yang, P. Sarkar, M. Barboiu, C. Y. Tang, and A. G. Fane, "Next-generation desalination membranes empowered by novel materials: Where are we now?" Nano-Micro Lett. **17**, 91 (2024).
[16]I. Ali, S. Z. Hasan, H. Garcia, and M. K. Danquah, "Recent advances in graphene-based nano-membranes for desalination," Chem. Eng. J **483**, 149108 (2024).
[17]S. Foorginezhad, M. M. Zerafat, A. F. Ismail, and P. S. Goh, "Emerging membrane technologies for sustainable water treatment: a review on recent advances," Env. Sci. Adv **4**, 530–570 (2025).
[18]H. R. Corti, G. A. Appignanesi, M. C. Barbosa, J. R. Bordin, C. Calero, G. Camisasca, M. D. Elola, G. Franzese, P. Gallo, A. Hassanali, K. Huang, D. Laria, C. A. Menendez, J. M. M. de Oca, M. P. Longinotti, J. Rodriguez, M. Rovere, D. Scherlis, and I. Szleiger, "Structure and dynamics of nanoconfined water and aqueous solutions," Eur. Phys. J. E **44**, 136 (2021).
[19]M. H. Köhler, J. R. Bordin, and M. C. Barbosa, "Ion flocculation in water: From bulk to nanoporous membrane desalination," J. Mol. Liq. **277**, 516–521 (2019).
[20]J. P. K. Abal, J. R. Bordin, and M. C. Barbosa, "Salt parameterization can drastically affect the results from classical atomistic simulations of water desalination by mos_2 nanopores," Phys. Chem. Chem. Phys. **22**, 11053 (2020).
[21]J. P. K. Abal and M. C. Barbosa, "Molecular fluid flow in mos_2 nanoporous membranes and hydrodynamics interactions," J. Chem. Phys. **154**, 134506 (2021).
[22]J. P. K. Abal, R. F. Dillenburg, M. H. Köhler, and M. C. Barbosa, "Molecular dynamics simulations of water anchored in multilayered nanoporous mos_2 membranes: Implications for desalination," ACS Appl. Nano Mater. **4**, 10467–10476 (2021).
[23]J. P. K. Abal and M. C. Barbosa, "Water mobility in mos_2 nanopores: effects of the dipole–dipole interaction on the physics of fluid transport," Phys. Chem. Chem. Phys. **23**, 12075 (2021).
[24]S. Homaeigohar and M. Elbahri, "Graphene membranes for water desalination," NPG Asia Mater. **9**, e427 (2017).
[25]Y. Li, Z. Xu, S. Liu, J. Zhang, and X. Yang, "Molecular simulation of reverse osmosis for heavy metal ions using functionalized nanoporous graphenes," Comput. Mater. Sci. **129**, 65–74 (2017).
[26]D. Cohen-Tanugi and J. C. Grossman, "Water desalination across nanoporous graphene," Nano Lett. **12**, 3602 (2012).
[27]D. Stauffer, N. Dragneva, W. B. Floriano, R. C. Mawhinney, G. Fanchini, S. French, and O. Rubel, "An atomic charge model for graphene oxide for exploring its bioadhesive properties in explicit water," J. Chem. Phys. **141**, 044705 (2014).
[28]Y. You, V. Sahajwalla, M. Yoshimura, and R. K. Joshi, "Graphene and graphene oxide for desalination," Nanoscale **8**, 117–119 (2016).
[29]Y. Yu, X. Xie, and S. Tang, "Molecular dynamics investigation on seawater desalination mechanism driven by external pressure through porous graphene membranes," J. Mol. Liq. **387**, 122595 (2023).
[30]H. H. I. Eltigani and Y. Boonyongmaneerat, "Progress of water desalination applications based on wettability and surface characteristics of graphene and graphene oxide: A review," Journal of Metals, Materials and Minerals **32**, 15–26 (2022).
[31]Y. Wang, Z. Je, K. M. Gupta, Q. Shi, and R. Lu, "Molecular dynamics study on water desalination through functionalized nanoporous graphene," Carbon **116**, 120 (2017).
[32]M. Hosseini, J. Azamat, and H. Erfan-Niya, "Improving the performance of water desalination through ultra-permeable functionalized nanoporous graphene oxide membrane," Appl. Surf. Sci. **427**, 1000–1008 (2018).
[33]G. Hummer, J. C. Rasaiah, and J. P. Noworyta, "Water conduction through the hydrophobic channel of a carbon nanotube," Nature **188**, 188 (2001).
[34]M. Dahanayaka, B. Liu, Z. Hu, Q. Pei, Z. Chen, A. W. Law, and K. Zhou, "Graphene membranes with nanoslits for seawater desalination via forward osmosis," Phys. Chem. Chem. Phys **45**, 19 (2017).
[35]M. H. Köhler, J. R. Bordin, and M. C. Barbosa, "2d nanoporous membrane for cation removal from water: Effects of ionic valence, membrane hydrophobicity, and pore size," J. Chem. Phys. **148**, 222804 (2018).
[36]R. F. Dillenburg, J. P. K. Abal, and M. C. Barbosa, "Computational investigation on water and ion transport in mos_2 nanoporous membranes: Implications for water desalination," ACS Appl. Nano Mater. **6**, 4465–4476 (2023).
[37]T. Yamada and R. Matsuzaki, "Efects of slit width on water permeation through graphene membrane by molecular dynamics simulations," Sci. Rep. **8**, 339 (2018).
[38]P. R. B. C. , M. B. Leão, G. L. R. Reis, D. D. de Vargas, G. F. Murillo, M. H. Köhler, and C. F. M. Jauris, "Unraveling the phosphorus adsorption mechanisms in threedimensional reduced graphene oxide materials," Langmuir **40**, 11173–11183 (2024).
[39]E. Y. Ang, T. Y. Ng, J. Yeo, Z. Liu, and K. Geethalakshmi, "Free-standing graphene slit membrane for enhanced desalination," Carbon **110**, 350–355 (2016).
[40]X. Xu, C. Lu, Y. Zhang, S. Li, Y. Yu, J. Zhao, and N. Wei, "Water desalination through charged graphene nanoslits: Role of edge chirality and electrostatic effects," Colloids Surf. A Physicochem. Eng. Asp. **725**, 137653 (2025).
[41]X. Yang and X. Yang, "Molecular simulation of water permeation and salt rejection for mos_2 nanoslit membranes," Desalination **564**, 116787 (2023).
[42]M. Liu, P. J. Weston, and R. H. Hurt, "Controlling nanochannel orientation and dimensions in graphene-based nanofluidic membranes," Nature communications **12**, 507 (2021).
[43]G. C., G. W. A. T., B. M. L., L. D. G., and M. P. V. E., "Exploring the pore charge dependence of k^+ and cl^- permeation across a graphene monolayer: a molecular dynamics study," RSC Adv. **9**, 20402 (2019).
[44]M. A., L. P., G. S., M. S. M., L. R., Z. J. M., B. Q., A. M., B. M., H. P., F. M., and M. D., "Colossal effect of nanopore surface ionic charge on the dynamics of confined water," J. Phys. Chem. **129 (40)**, 18311–18324 (2025).
[45]S. Liu, Z. Foo, J. Lienhard, S. Keten, and R. Lueptow, "Membrane charge effects on solute transport in nanofiltration: Experiments and molecular dynamics simulations," Membranes **15**, 184 (2025).
[46]R. Fuentes-Azcatl and M. C. Barbosa, "Sodium chloride, $nacl/\varepsilon$: New force field," J. Phys. Chem. B. **120**, 2460 (2016).
[47]A. P. Thompson, H. M. Aktulga, R. Berger, D. S. Bolintineanu, W. M. Brown, P. S. Crozier, P. J. in 't Veld, A. Kohlmeyer, S. G. Moore, T. D. Nguyen, R. Shan, M. J. Stevens, J. Tranchida, C. Trott, and S. J. Plimpton, "Lammps - a flexible simulation tool for particle-based materials modeling at the atomic, meso, and continuum scales," Comp. Phys. Comm. **271**, 108171 (2022).
[48]D. Frenkel and B. Smit, *Understanding Molecular Simulation - From Algorithms to Applications*, Vol. Second Edition (Academic Press, 2002).
[49]S. Nosé, "A molecular dynamics method for simulations in the canonical ensemble," Mol. Phys. **52**, 255 (1984).
[50]W. G. Hoover, Phys. Rev. A: At., Mol., Opt. Phys. **31**, 1695 (1985).
[51]H. J. C. Berendsen, J. R. Grigera, and T. P. Straatsma, "The missing term in effective pair potentials," J. Phys. Chem. **91**, 6269 (1987).
[52]X. Yang and X. Yang, "100 years of the lennard-jones potential," J. Chem. Theory Comput. **20**, 3379–3405 (2024).
[53]B. A. Luty and W. F. van Gunteren, "Calculating electrostatic interactions using the particle-particle particle-mesh method with nonperiodic long-range interactions," J. Phys. Chem. **100**, 2581–2587 (1996).
[54]Q. Zhang, X. Wang, J. Li, and D. Lu, "How pressure affects confine water inside different nanoslits," RSC Adv. **9**, 19086 (2019).

[55]M. H. Köhler, J. R. Bordin, C. F. de Matos, and M. C. Barbosa, "Water in nanotubes: The surface effect," Chem. Eng. Sci. **203**, 54–67 (2019).

[56]B. Roux, "The calculation of the potential of mean force using computer simulations," Comput. Phys. Commun. **91**, 275–282 (1995).